UNIVERSITY OF CALIFORNIA

Radiation Laboratory

BERKELEY, CALIFORNIA

DISCLAIMER

COPY 2

UCRL 326

UNIVERSITY OF CALIFORNIA

Radiation Laboratory

Contract No. W-7405-eng-48

FOR OFFICIAL USE ONLY

UNCLASSIFIED

SUMMARY OF THE RESEARCH PROGRESS MEETING

March 24, 1949

H. P. Kramer

Berkeley, California

INSTALLATION	NO. COPIES
Argonne National Laboratory	10
Armed Forces Special Weapons Project	1
Atomic Energy Commission, Washington	2
Battelle Memorial Institute	1
Brookhaven National Laboratory	10
Bureau of Ships	1
Carbide & Carbon Chemicals Corporation (K-25)	4
Carbide & Carbon Chemicals Corporation (Y-12)	4
Chicago Operations Office	8
Columbia University (Dunning)	1
Columbia University (Failla)	1
General Electric Company, Richland	7
Hanford Operations Office	8
Iowa State College	1
Kellex Corporation	2
Knolls Atomic Power Laboratory	4
Los Alamos	6
Massachusetts Institute of Technology (Gaudin)	1
Massachusetts Institute of Technology (Kaufmann)	1
Mound Laboratory	8
National Advisory Committee for Aeronautics	2
National Bureau of Standards	2
Naval Radiological Defense Laboratory	2
NEPA Project	1
New York Operations Office	8
North American Aviation, Inc.	2
Oak Ridge National Laboratory	12
Patent Advisor, Washington	1
Sandia Base	2
Technical Information Branch, ORE	15
UCLA Medical Research Laboratory (Warren)	1
University of California Radiation Laboratory	6
University of Rochester	2
Western Reserve University (Friedell)	4
Sylvania Electric Products, Inc.	1

INFORMATION DIVISION
Radiation Laboratory
Univ. of California
Berkeley, California

SUMMARY OF THE RESEARCH PROGRESS MEETING

March 24, 1949

H. P. Kramer

N-p Scattering at 280 Mev. C. Leith.

Previous n-p scattering measurements at 40 mev and 90 mev have been continued at 280 mev. The same apparatus has been used throughout. (Fig. 1) A collimated neutron beam scatters protons from a sheet of paraffin, carbon, or polystyrene. These protons are registered in a telescope of three counters in coincidence. Energy control is achieved by means of a tungsten absorber placed between the second and third counter. In order to minimize the loss of protons that are scattered in the absorber, the absorber is placed as close as possible to the third counter which has a somewhat larger cross section than the preceding two.

Fig. 2 shows the differential scattering cross section for neutrons at 40 mev, 90 mev and 280 mev. The curve for 280 mev neutrons is rather uncertain. At the low scatter angle end of the curve it may be displaced by as much as 15 percent. According to theory, one would expect the curve for 280 mev neutrons to have a steeper slope at small angles than is shown in the graph.

A crude energy distribution has been found for the incident neutrons. (Fig. 3) No values are given for energies below 200 mev since the absorber does not permit recoil protons with energies less than 200 mev to penetrate to the third counter.

Some of the particles that possess an energy in excess of the loss of energy due to ionization in the absorber do not reach the third counter because of nuclear absorption. Since the rate of energy loss by ionization varies inversely as the energy, one must use a greater thickness of absorber at small scatter angles than at large angles in order to achieve the same cut-off energy E_o in both cases. For this reason, the loss of protons in the absorber through nuclear capture is greater

at small angles between the line of the telescope of counters and the incident neutron beam than it is for large angles. At 10° it is necessary to add at least 25 percent of the measured number of coincidences to this number in order to arrive at the number of protons with energy greater than E_o that are scattered at 10°. At 45° a correction of only 10 percent is necessary.

Measurements with the present apparatus will be extended to a 75° scatter angle.

Distribution of Radiation from the Synchrotron. E. McMillan.

In an effort to account for all of the radiation produced in the synchrotron measurements have been made with electroscopes at a number of points outside of the machine. The radiation can be grouped into three classes: that which is contained in the beam, that which is produced by electrons that are sprayed tangentially from the orbit and produce radiation that can be compared to the spray coming from a water wheel, and finally radiation that is produced by electrons that are scattered through large angles in the target.

The plot of the intensity of the x-ray beam is a bell-shaped curve. The intensity decreases to 1/10 of maximum on both sides of the peak. This is, however, still above the intensity of the spray which is uniform around the machine. The intensity of the beam without the uniform background is plotted on a logarithmic scale in Fig. 4. The dotted line represents the results of a calculation made by Schiff by considering scattering in the target and the mechanism of beam production.

Although the deviation of the theoretical results from the experimental values is so small that it would be impossible to observe it on a non-logarithmic scale it is nevertheless real.

Two different explanations for this deviation have been advanced. One of these states that since the theoretical curve is based on the proportionality of scattering to the square root of the thickness of target traversed by an electron and since a

uniform value of 1/2 mm. was used in the calculations for the thickness of the target, the divergence of the theoretical value from the experimental results is probably due to those electrons which traverse the target at slightly different angles and thus pass through greater thicknesses of material. The second explanation, on the other hand, implies that the difference between theory and experiment would exist even if the assumed target thickness were correct for all electrons, and attributes it to scattering.

Fig. 5 shows the distribution of radiation from the synchrotron. The "bump" in the intensity consists of the x-rays that are emitted from the plastic tank wall by electrons scattered from the target through more than 45°. If one assigns the value 1 to the intensity of radiation in the beam, and in all cases multiplies the intensity by the effective area over which it exists in order to calculate the flux, one obtains a table such as the following in which the total radiation from the synchrotron is accounted for.

	Intensity	Effective Area	Flux	% of Total
Spray	.0015	2000 sq. in.	3	59%
Bump	.005	200 sq. in.	1	20%
Beam				
theoretical	1	.76 sq in.	.76	15%
experimental excess		.37 sq. in	.37	7%

Effective area in this table means the area around the synchrotron where the intensity has approximately the listed value. The flux in the beam is calculated by evaluating the integral flux = $2\pi \int I\, r\, dr$ graphically by means of Fig. 4.

Ordinary radiation theory states that 14 percent of the energy of the electrons that impinge on a 1/2 mm. target is emitted in the form of an x-ray beam. The

value of 15 percent which refers to the production of x-rays in an ideal 1/2 mm. target is in good agreement with the theory.

All electrons that traverse the target lose at least 1 mev of their energy and therefore drop to a radius 1 cm. smaller than the radius of maximum energy. At the new radius they are no longer stable and thus may fly off to hit some portion of the apparatus and produce what has been tabulated as the spray. Since this is emitted at random, it is uniformly distributed around the machine.

The possibility was considered that the low intensity spread in the beam might be caused by secondaries from the quartz wall and other solid pieces of the apparatus through which the beam must pass. Tungsten wires were placed in the beam which was photographed on x-ray film. It was seen that the intensity of the shadows that were cast by the tungsten wires was uniform throughout the beam and it was concluded that all quanta came from the same source and hence could not have been produced by secondary processes.

Metabolism of Some Simple Carbon Compounds. H. Jones.

Some of the carbon compounds that have been synthesized by M. Calvin's group have been used to perform metabolism studies on mice. Fig. 6 shows the apparatus that allows one to measure the rate of consumption and to judge the manner of consumption by the body cells of these compounds. The mouse is contained in a closed system: its intake and elimination are completely controlled. Atoms of radioactive carbon are substituted for the inert atoms in various positions in the molecules of the organic compounds which are then introduced into the body of the mouse by injection into the tail vein. After a short lapse of time, the radioactive carbon appears in the CO_2 that is exhaled by the animal. By counting the number of radioactive atoms that are exhaled and plotting this quantity against the time one is able to observe the rate of consumption of the organic compound and its constituents, that is, one forms a quantitative idea of the metabolism of the animal, since

the rate of exhalation of $\overset{*}{C}O_2$ is proportional to the total amount of labeled carbon that is present in the body.

In order to obtain the result that the exhalation of CO_2 is proportional to the amount of CO_2 that is present in the body, the mouse was allowed to breathe air that contained a fixed amount of labeled oxygen. The graph of Fig. 7, shows the timewise decay of the number of counts observed in the CO_2 that was exhaled.

When acetic acid, CH_3C^*OOH, is injected into the mouse, and the radioactivity of the exhaled CO_2 is counted one obtains the variation of values that is depicted in Fig. 8. When this curve is resolved one finds that one is dealing with three process whose half-lives are 10 min., 60 min., and 7 hrs. The half life in this context means the interval of time during which the count decreases by a factor of 1/2. A similar decay curve was observed when the labeled atom was shifted from the methyl to the carboxyl position, i.e. when C^*H_3COOH was used. The rates of consumption were the same. The quantity of CO_2 that was exhaled was however twice the amount that was previously observed.

When glycine, $CH_2NH_2\overset{*}{C}OOH$, was administered the decay curve of Fig. 9 resulted. Upon resolution the curve shows three different components of half-lives 13-14 min., 62 min., and about 10 hrs. Each component points to a different manner of consumption of the injected quantity of compound. When the label is shifted to the first carbon position, that is when C^*HNH_2COOH is used, an entirely different behaviour is observed. Fig. 10 shows four half-lives of 3 min., 10 min., 80 min., and 10 hrs. It is planned to study the metabolism of this compound more closely.

Formic acid, HCOOH, which is generally considered a toxic agent and is not normally consumed by mammalian tissue was next studied. The graph of Fig. 11 shows half-lives of 9.2 min., 30-35 min., and 10 hrs. It is seen that this compound moved into the intermediate metabolism stage as rapidly as the more nutritious ones.

Since the presence of a cancer in an animal has a profound effect on its metabolism the techniques that have been described can be used to good advantage in making a comparison in particular of the carbon metabolism of cancerous and normal animals. Seventy healthy and 20 cancerous animals were fed propionic acid, $CH_3C^*H_2COOH$, and it was found that the metabolism was actually different for the diseased mice than for the healthy ones. The results are shown in Fig. 12. The time constants, half-elimination times, are compared in the following table:

	C_1	C_2	C_3
Normal mice	6.08 ± 1.0 min.	29.5 min.	15 hrs.
Cancerous mice	7.05 ± 1.0 min.	28.8 min.	15 hrs.

The label was shifted to the first position, and the substance, $C^*H_3CH_2COOH$ was administered to 15 tumorous and 15 healthy animals. A comparison of the three time constants does not indicate a pronounced difference in the consumption.

Fig. 13 shows a similar comparison for the metabolism of pyruvic acid. The time constants are:

	C_1	C_2	C_3
Normal	8.2 min.	32 min.	13 hrs.
Tumorous	8.2 min.	34 min.	13 hrs.

Although the ultimate aim of these studies is to enable the biologist and biochemist to predict the course through the body of any simple carbon compound the research has not advanced sufficiently at present to make this possible.

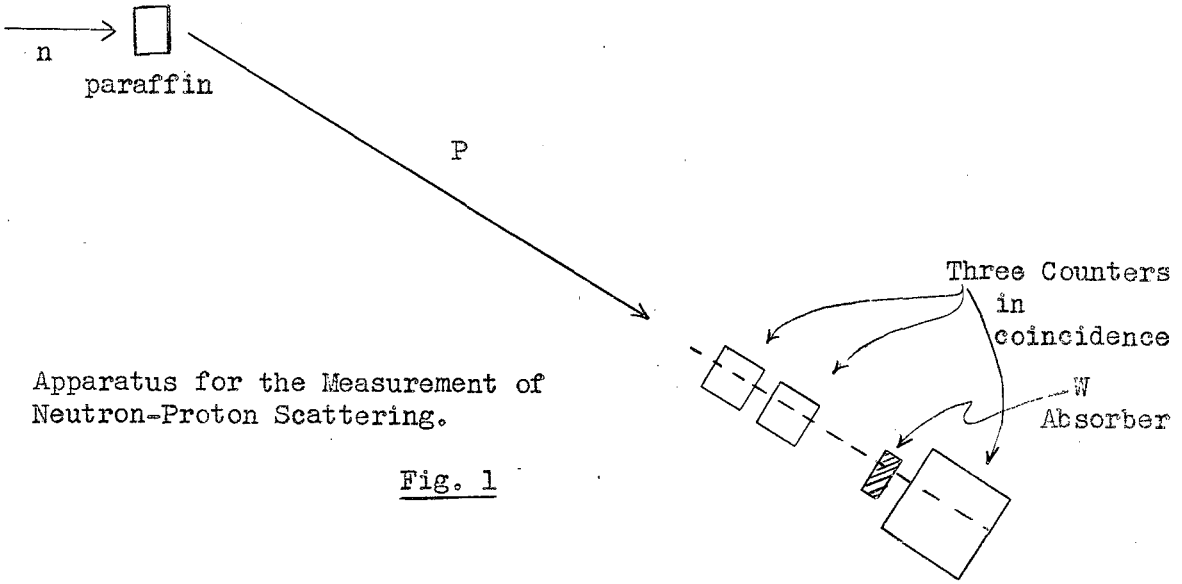

Apparatus for the Measurement of Neutron-Proton Scattering.

Fig. 1

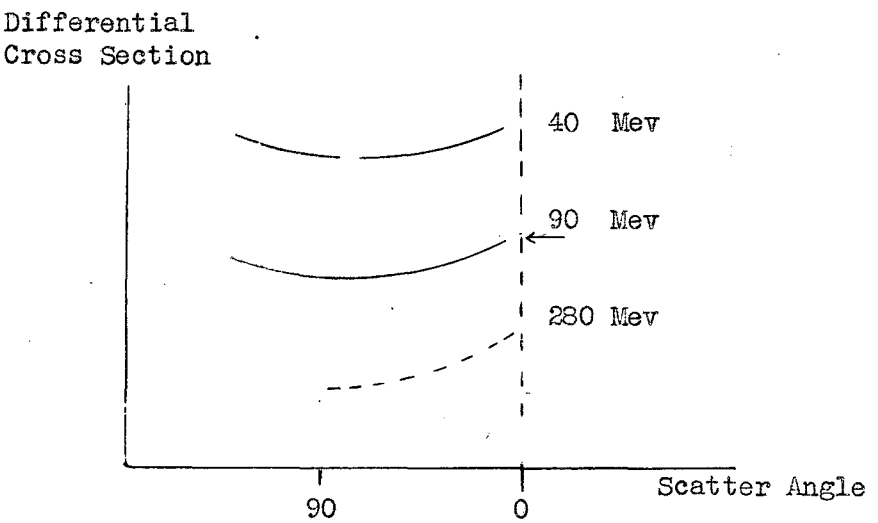

Fig. 2

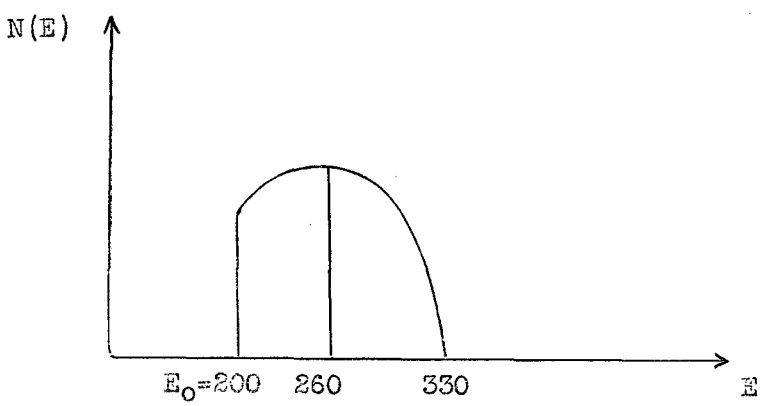

Energy Distribution of 280 Mev Neutrons

Fig. 3

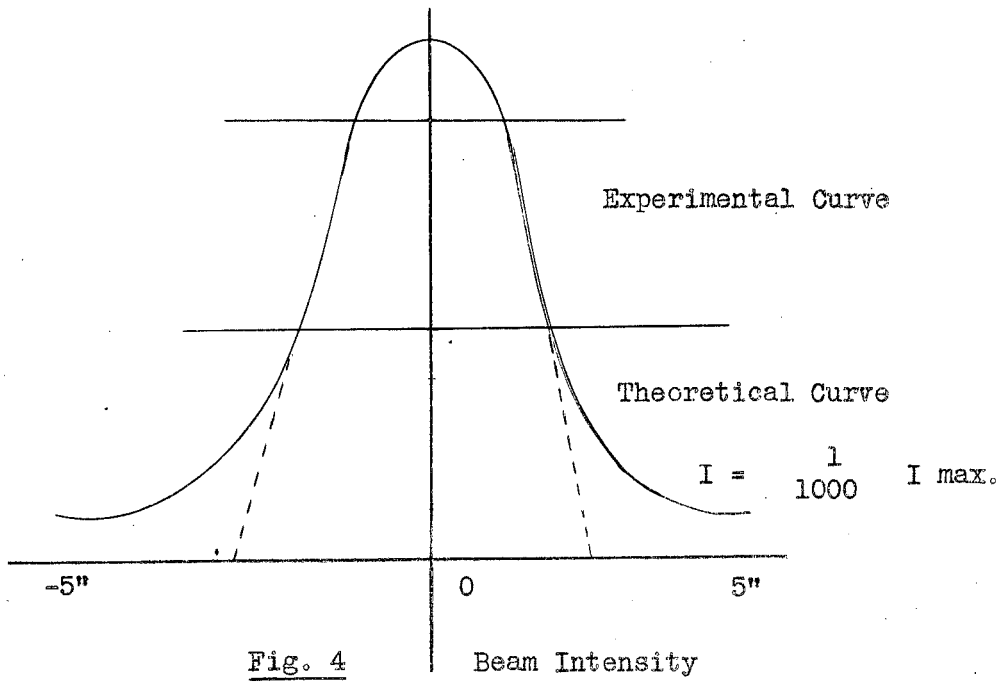

Fig. 4

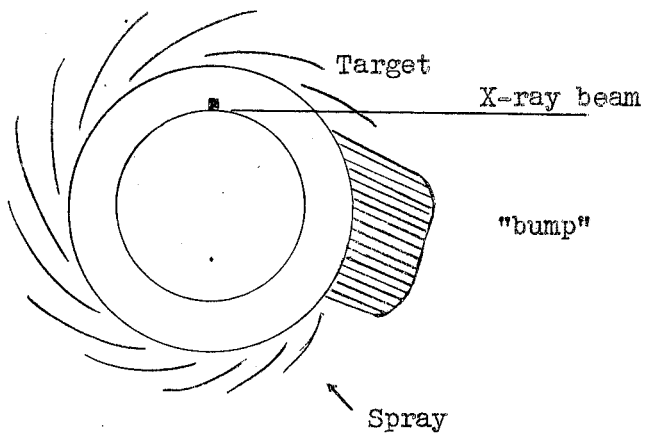

Distribution of Radiation Around the Synchrotron.

Fig. 5

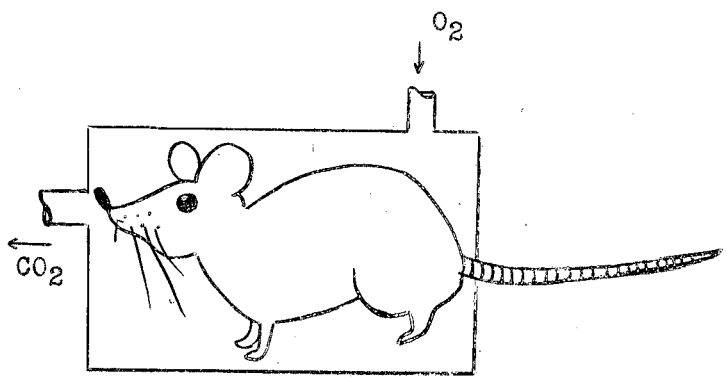

Mouse Holder for Metabolism Studies

Fig. 6

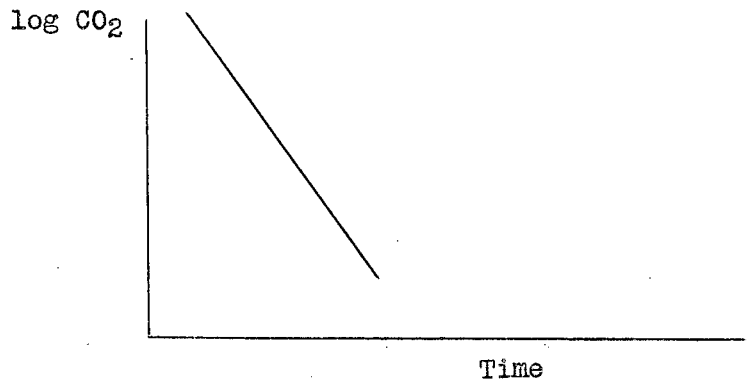

The Rate of Exhalation of CO_2 is Proportional to the Amount Present in the Body.

Fig. 7

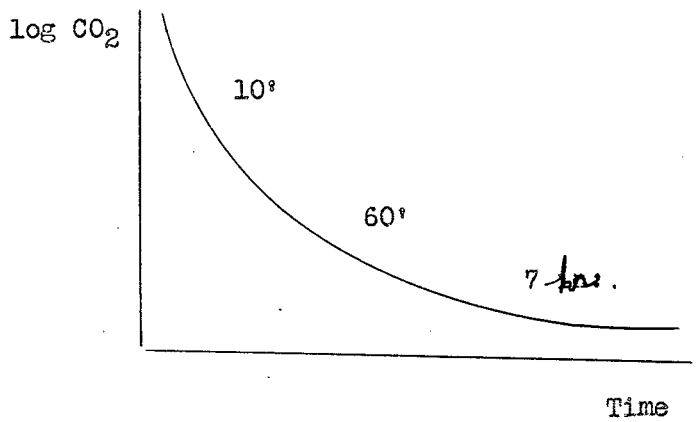

Exhalation of $\overset{*}{C}O_2$ After Injection of CH_2C^*OOH

Fig. 8

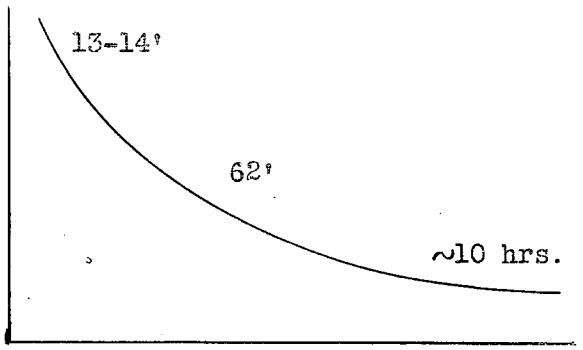

Exhalation of C^*O_2 After Injection of $CHNH_2C^*OOH$

Fig. 9

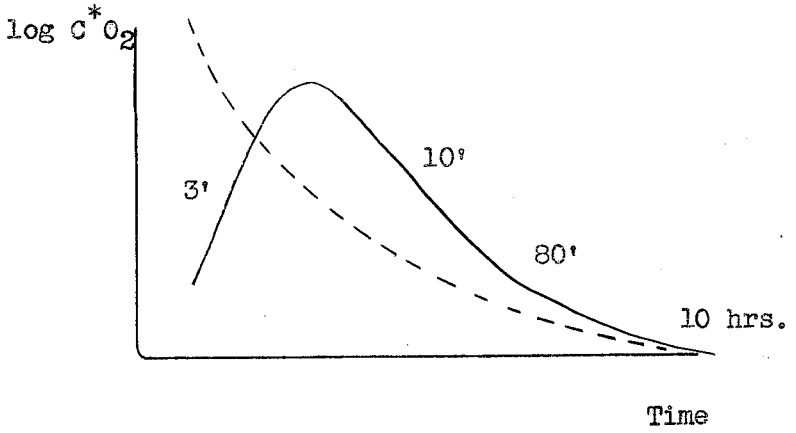

Exhalation of C^*O_2 After Injection of $C^*HNH_2C^*OOH$

Fig. 10

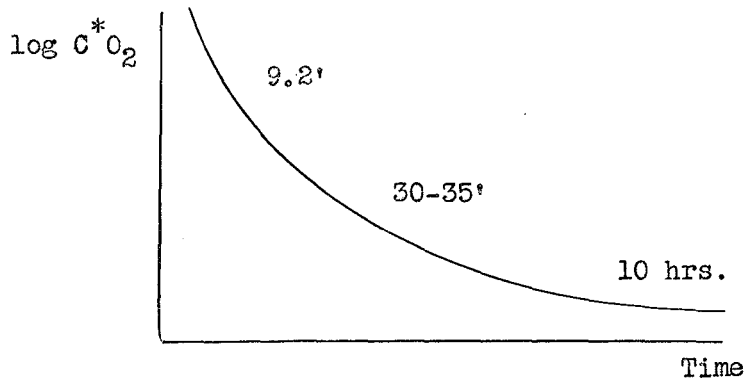

Exhalation of C^*O_2, After Injection of HC^*OOH

Fig. 11

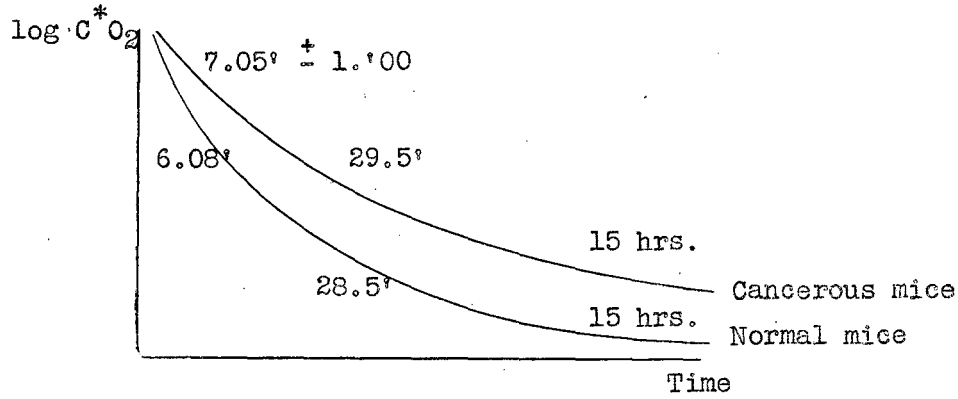

Fig. 12

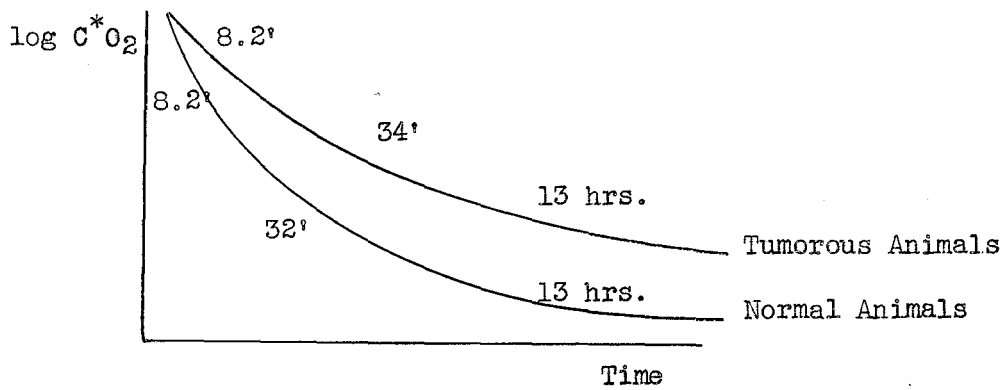

Fig. 13